京都大学防災研究所年報 第 65 号 B
DPRI Annuals, No. 65 B, 2022

Preliminary Investigation of Change of Snake Line Pattern Based on Clausius-Clapeyron Relation

Ying-Hsin WU, Eiichi NAKAKITA and Akihiko YAMAJI

Synopsis

The impact of climate change on sediment hazard occurrence is urgently needed to resolve for pursuing the future sustainable living environment. To this end, this research aims to propose a new approach to physically quantify the change of snake line patterns with the application of Clausius-Clapeyron scaling law. The key of the proposed approach is to establish the physically based linkage among air temperature change on ground surface, peak precipitation intensity, and corresponding snake line pattern of certain percentiles of rainfall events. In this study, we used 99th and 50th percentiles for representing extreme and general precipitation conditions. With the long-term meteorological observation at Kobe meteorological observatory, we successfully verified the applicability of the proposed approach on identifying the change of snake line pattern. The regional climate projections of 5-km NHRCM were then analyzed to examine the future change of Clausius-Clapeyron scaling in the Japanese archipelago. Meanwhile, we also revealed the future change of snake line patterns under climate change influences.

Keywords: Clausius-Clapeyron scaling, snake line, climate change, NHRCM

1. Introduction

Extreme climate have become more and more frequent to bring considerable severe water-related disasters world-wide. Beyond our past experience, recent extreme rainfall events in Japan show some evident changes that rainfall seems to be elongated in the period and intensified in a much higher accumulated amount and peak intensity. The extreme rainfall has broken new observation records locally in many places, and consequently triggered numerous devastating floods, inundation, landslides and sediment disasters. Among relevant influential factors, extreme weather could be attributed to the global warming phenomenon which exhibits an average temperature rise on earth sur-face due to human activities of rapid industrial development in the last century. The long-term heating process of global warming phenomena seems to continuously alter atmosphere for a longer period to enhance weather more extreme in the strength and more often than the past in near future. Assessment of climate change impact on our living environment is urgent and necessary for pursuing a safer and sustainable living environment.

More extreme precipitation may cause more flooding and sediment disasters which critically threaten our life and living environment. Assessment of extreme rainfall and its impact on relating disasters have been an active research theme in recent decades (e.g., Utsumi et al., 2011; Westra et al., 2014; Nakakita et al., 2018; Mori et al., 2021; Nakakita et al., 2021; Hayashi et al., 2022). To identify the impact of climate change on sediment disasters, some efforts (Wu et al., 2020; Wu et al., 2021) have been made for identifying rainfall prone to sediment hazards using the critical line method (Osanai et al., 2010), which is currently applying by Ministry of Land, Infra-structure, Transport and Tourism (abbreviated as MLIT) for robust early-

warning of landslides and sediment disasters in Japan. The critical line method uses a parametric curve of snake line, consisting of two hydro-meteorological parameters of hourly rainfall intensity (hereafter defined as *P*) and soil-water index (abbreviated as *SWI*), to reflect long and short-term rainfall influences. Until now, it still remains an unresolved puzzle for the early-warning of sediment disaster in a changing climate using the current methodology. Therefore, we are trying to develop a new approach to physically quantify climate change impacts on snake line patterns by utilizing the variable of air temperature on ground surface. To this end, we utilized Clausius-Clapeyron (CC) scaling to identify the change rate of precipitation intensity of certain percentile in terms of air temperature change, and then utilized the representative rainfall events identified in the CC scaling analysis to obtain corresponding maximum *SWI* of each event. With all collected pairs of representative *SWI* and *P*, linear regression analysis was performed to obtain a scaling relation of snake line for interpretation of the change rate of *SWI* using air temperature change. With the application of atmospheric thermodynamics, this new approach intends to quantify the relative change of *SWI* and *P* once given any air temperate change. Analysis of historical gauge observation and regional climate projections were performed for investigating the applicability of the proposed approach. As a major merit, the key motivation of this research aims to propose a physically based approach to estimate the change of snake line patterns, or says the future tendency of sediment hazard, in terms of air temperature change under climate change influences.

2. Data and Method

2.1 Observation at Kobe Meteorological Station

To verify our approach, we used the historical observation of precipitation, air temperature and dewpoint temperature recorded by the ground gauge at the weather station of Kobe Meteorological Observatory, which is currently operating by Japan Meteorological Agency (JMA). The dataset period ranges from 1990 to 2019 of which is 30 years in total, and the time resolution is one hour.

2.2 Climate Projections: 5-km NHRCM

We used the climate projections of 5-km Non-Hydrostatic Regional Climate Models (abbreviated as RCM5), which are developed and published by Meteorological Research Institute of JMA. The spatiotemporal resolution of RCM5 is 5 km in space and 30 minutes in time, and the simulation domain consists of totally 527×804 grids to cover the whole Japan archipelago. As are tabulated in Table 1, six members include SPA for present climate, and the others (SFA_26, SFA_c0, SFA_c1, SFA_c2, and SFA_c3) for future climate under the scenarios of Representative Concentration Pathway 2.6 and 8.5, abbreviated as RCP2.6 and RCP8.5, which are proposed in IPCC Fifth Assessment Report in 2014 to reflect human activities of industrial development. RCP8.6 and RCP2.6 can be regarded as the scenarios under the temperature increase of 4℃ and 2℃, respectively due to the human activities of industrial development. The domain boundary conditions for RCM5 are derived from the global climate simulations using MRI-AGCM3.2S (Murata et al., 2015). For the RCP8.5 scenario, four spatial patterns

Table 1 Brief information of all 5-km NHRCM members

Dataset	Scenario	Boundary condition of SST†	Simulation Period
SPA	-	Monthly observation (1979-2003)	from 1980/09/01 to 2000/08/30
SFA_26	RCP2.6	El Niño	from 2076/09/01 to 2095/08/30
SFA_c1	RCP8.5	Less warmer in East tropical Pacific	
SFA_c2	RCP8.5	Stronger El Niño	
SFA_c3	RCP8.5	Warmer in Northwest Pacific	
SFA_c0	RCP8.5	El Niño	

†SST: Sea surface temperature

Table 2　5-km NHRCM surface parameters for analysis

Parameter	Variable name & description	Unit
SMQR	accumulated precipitation of liquid water	[mm]
U	*x*-direction wind velocity on the ground surface	[m/s]
V	*y*-direction wind velocity on the ground surface	[m/s]
T	surface air temperature	[K]
TTD	surface dewpoint depression	[K]
TPW	total precipitable water	[mm/hour]

of sea-surface temperature, or says SST, are imposed as the sea surface boundary conditions for projection simulations. The simulation period of each dataset is 20 years with a one-year time slice and a spin-up period of 43 days. More details about RCM5 can refer to the literature (Sasaki et al., 2012). Table 2 lists six parameters which will be used in this analysis. All parameters are directly extracted without interpolation. Particularly, we averaged the four ensemble members of the scenario RCP85 (SFA_c0, SFA_c1, SFA_c2, and SFA_c3) to focus on discussing the average features.

2.3 Clausius-Clapeyron Scaling of Precipitation

One of the conventional way to interpret the relation between atmospheric temperature and extreme precipitation is the famous Clausius-Clapeyron relation. For the application of the relation, an exponential based scaling can be approximately expressed as (Utsumi et al., 2011, Nayak et al., 2018),

$$P_{r2} = P_{r1}(1+\alpha)^{\Delta T}, \text{ for } \Delta T = T_{r2} - T_{r1}, \quad (1)$$

where the subscripts *r*1 and *r*2 denote two rainfall events; *P* and *T* are precipitation and air temperature on the ground surface, respectively. α is the rate of change of precipitation, and $\alpha \approx 6.8$ %/℃ at 25 ℃. In general a constant CC scaling is determined through regression analysis on logarithm of precipitation intensity of certain percentiles with respect to temperature or dewpoint temperature. In literature, daily maximum precipitation and temperature have been widely used to interpret relationship between atmospheric condition and extreme precipitation. Differently, we herein are attempting to investigate constant CC scaling law in terms of maximum hourly precipitation and temperature of given rainfall events. For significant analysis the procedures are briefly explained. We first followed the official MLIT guideline (MLIT, 2009) to extract all representative rainfall events. All extracted events are classified into 10 bins of equal event numbers. The main reason to use 10 bins to guarantee that there are at least more than 100 events in each bin. Then, in each bin, the median value of temperature is extracted as the representative temperature, and hourly precipitation intensity are ranked to determine the 99-th and 50-th percentiles, i.e., P_{99} and P_{50}, for representing extreme and general precipitation conditions, respectively. Finally, all extracted representative temperature and precipitation of different percentiles are used for determining corresponding CC scaling.

To remind, a constant CC scaling of precipitation intensity may break at up to certain temperature because of more atmospheric destabilizing forcings entering into precipitation process in mid-attitudes (Westra et al., 2014). Being called peak-point temperature (Utsumi et al., 2011), or says *PPT*, this threshold varies from place to place in terms of many influential factors. It is beyond the main interest of the present analysis to investigate the influential factors for *PPT*, but we shall identify the value through the way as mentioned in the following. Therefore, as a reasonable way, this analysis also intends to possibly find out the *PPT* by detecting the temperature point where the slope gradient of the smoothed curve using the method of locally-weighted regression smoothing (Utsumi et al., 2011) diverges from the original change CC scaling rate α. To remind here, the determination of *PPT* is only

based on mathematically analyzing the curves obtained by applying weighted regression smoothing to all data pairs of representative precipitation and air temperature.

2.4 Procedures for 5-km NHRCM analysis

In this study, the six parameters to analyze are listed in Table 2. The time series of each parameter on each 3rd MLIT mesh of which the spatial resolution is about 1 km^2 was directly extracted without any interpolation. We set 0.5 mm/hr as the minimal threshold of precipitation rate to exclude the data in the time series of precipitation in the RCM5 datasets. The conventional methodology using a tank model proposed by JMA was applied to obtain the time series of *SWI*. As has been explained in the section of 2.3, the next step is to extract all representative rainfall events from the processed time series of precipitation by following the official guideline (MLIT, 2009), which is the same the way used for CC scaling analysis. We intend to know more atmospheric conditions during all extracted representative rainfall events, we also analyzed the other five parameters derived from RCM5. The data of dewpoint temperature T_d was straightforwardly derived by subtracting dewpoint depression *TTD* from surface air temperature *T*. Simultaneously, we extracted the total precipitable water *TPW* as another index to know how much atmospheric water vapor exists in any given effective rainfall event. Besides, to judge atmospheric stability condition, we further processed an additional parameter of horizontal divergence on ground surface, defined as

$$HDIV = \vec{\nabla}_h \cdot \left(\vec{U}_{sfc}\right), \tag{2}$$

where $\vec{\nabla}_h$ is the gradient operator with respect to the two horizontal coordinates of (x, y) and $\vec{U}_{sfc}$ are the wind velocities on the ground surface. For gradient operation, the spatial increment is set to be 5 km. As for the physical meaning, in terms of mass conservation of air flow motion, a greater negative value of *HDIV* represents higher net inflow of ambient air and consequentially turns into stronger vertical updraft which could destabilize atmosphere to generate precipitation. In each representative rainfall event, we extracted the minimum negative *HDIV*, the average of *TPW*, and maximum *T* and T_d to comprehensively understand the corresponding atmospheric conditions how likely generate rain for consequentially revealing the change of snake line patterns in terms of atmospheric influences.

2.5 Scaling of Change of Snake Lines

For the other target of the present analysis, we aim to recognize the relationship between changes of snake line patterns and atmospheric conditions. By taking the merit of the percentile concept in the analysis of CC scaling as well as the representative rainfall events, on each 3rd mesh we herein propose a new positively proportional relation between all representative *SWI* and *P* of any certain percentile.

A heuristic derivation is mentioned in the following. We first assume the change of snake line holds a scaling relation, i.e., a function of change ratio in terms of *SWI* and *P* of each rainfall event. Then, the snake line scaling β can be expressed as

$$\beta \approx f\left(\frac{SWI_i}{P_i}\right), \tag{3}$$

where $f(\cdot)$ denotes the function interpreting the change rate of *SWI* to *P* on each mesh, and the subscript i denotes the representative classification in the configuration of the present analysis. We next attempt to find the connection between CC scaling and snake line scaling. Let us consider that the *SWI* of the second rainfall event SWI_{r2} can be furthered represented by

$$SWI_{r2} \approx \beta \times P_{r2}, \tag{4}$$

Then, with the CC scaling in Equation (1), P_{r2} can be replaced by $P_{r1}(1+\alpha)^{\Delta T}$ to give

$$SWI_{r2} \approx \beta \times P_{r2} = \beta P_{r1}(1+\alpha)^{\Delta T}, \tag{5}$$

The above equation exhibits a relation that *SWI* can be positively proportional to β and $(1+\alpha)^{\Delta T}$, as below

$$SWI \approx \beta P \approx \beta(1+\alpha)^{\Delta T}, \tag{6}$$

where reasonably interprets the relative change ratio of soil-water index *SWI* to hourly precipitation *P* in term of CC scaling rate and air temperature change,

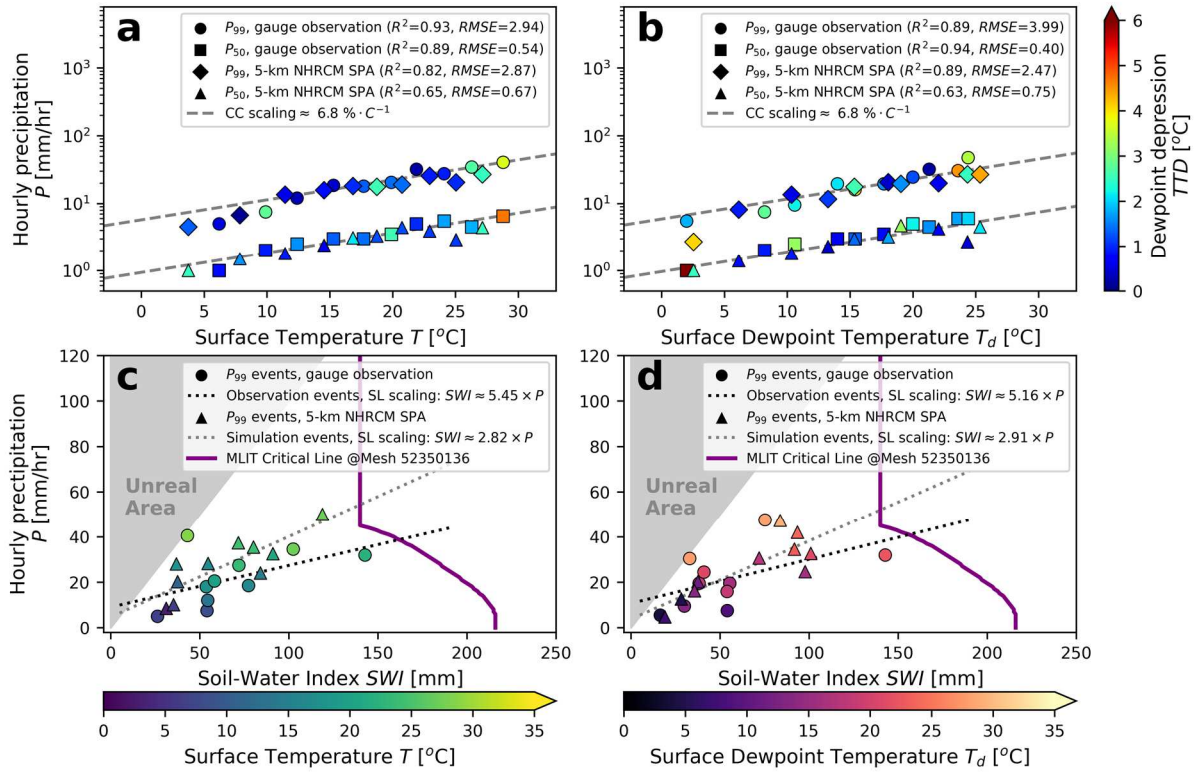

Fig. 1 Comparison of CC scaling of the 99-th and 50-th percentiles, i.e., P_{99} and P_{50}, between observation and 5-km NHRCM simulation at the mesh where JMA Kobe meteorological observatory is located. Surface temperature is used for a) and c); dewpoint temperature for b) and d). All symbols in c) and d) denote the pair of maximum hourly precipitation P and soil-water index SWI in the corresponding rainfall events of P_{99} and P_{50}, respectively.

which is a widely evident phenomenon in climate change. To remind here, the merit of the ratio of snake line change is to be able to assess the change of snake line pattern once given a temperature change due to any climate scenario or so on.

3 Results and Discussion

3.1 Comparison with Gauge Observation

Analysis were performed to verify the CC scaling laws in the 99-th and 50-th percentiles of precipitation obtained by observation and RCM5 simulation, and to investigate the corresponding parametric pairs of snake lines of the P_{99} events. Fig. 1 shows the comparison results. Both of surface air temperature T and dewpoint temperature T_d are used for determining the CC scaling. As a result, without obvious difference of change rate between the CC scaling using T and T_d, we hereafter chose temperature T for the following analysis. Also, it is obviously that the change rates of precipitation P_{99} and P_{50} obtained from historical observation and RCM5 simulation coincide with each other very well. This good agreement could indicate that RCM5 simulation can provide reasonable scaling of extreme and general precipitation. Regarding dewpoint depression, the result shows most of rainfall events occurred when the air temperature nearby ground surface was close to dewpoint temperature. However, some events occurred in higher surface temperature as well as high dewpoint depression. These events can refer to that some other atmospheric forcing got into precipitation generation, and they require more analysis with the help of atmosphere measurement to identify the real mechanism. Finally, as for the change of snake lines, the distribution of the pairs of maximum P and SWI of the P_{99} events shows that some pairs in higher temperature generally approach to the critical line denoting a threshold boundary of higher risk of

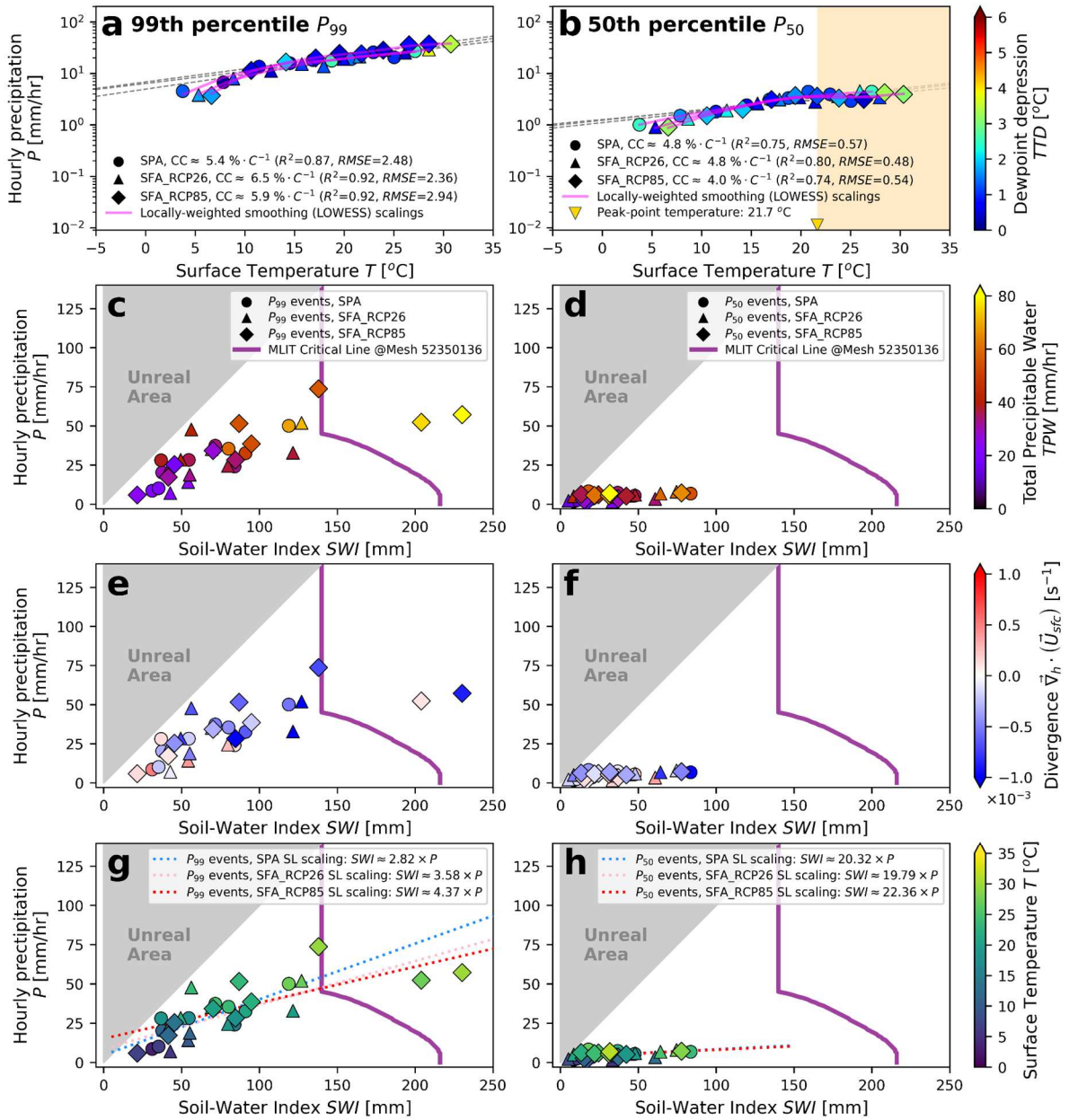

Fig 2 Comparison of RCM5 members in P_{99} and P_{50} events and the corresponding pairs of snake line in terms of c) and d) total precipitable water *TPW*; e) and f) surface horizontal divergence *HDIV*; g) and h) surface temperature *T*. The location is at JMA Kobe meteorological observatory. In P_{50} events, a peak-point temperature of 21.7 °C is detected by the clear change of slope gradient from the locally weighted smoothed curves of CC scaling, i.e., light purple curves in a) and b).

occurrence of sediment disasters (Osanai et al., 2010). From the snake-line scaling curves, we can infer the increasing trend of *SWI* with *P* is enhanced by any increment of temperature rise due to global warming. Then, it can be expected to estimate the corresponding change ratio β for the pattern of snake line, further representing the possible tendency of sediment disaster occurrence in a higher confidence.

3.2 Application to RCM5 members

Alongside the relationship among CC scaling and snake line scaling, we utilized two more surface parameters derived from RCM5 to know the atmospheric conditions during events. The additional two parameters are total precipitable water *TPW* and surface horizontal divergence *HDIV*, as expressed in Eq. (2). *TPW* can be referred to the

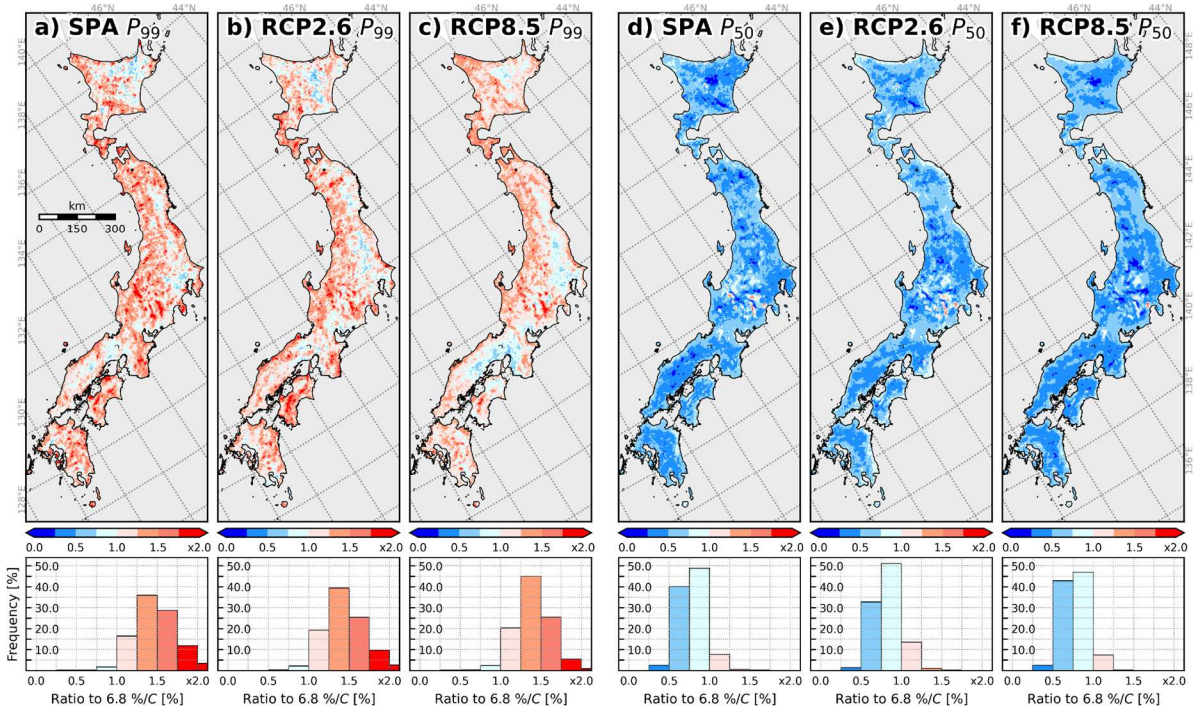

Fig. 3 Spatial and frequency distributions of rate of precipitation change α of CC scaling of P_{99} (subfigures a-c) and P_{50} events (d-f) from all members of 5-km NHRCM. The standard CC scaling of 6.8 %/℃ at 25 ℃ is used for normalization.

capacity of water vapor in the air for rainfall generation, and *HDIV* can help understand the atmospheric stability condition whether it may exist an updraft or not to contribute cumulonimbus and storm development. Fig. 2 shows the comparison results of P_{99} and P_{50} events from SPA for present climate, and SFA26 (RCP2.6 scenario) and SFA85 (RCP8.5 scenario) for future climate on the mesh where the Kobe meteorological observatory is located. In Fig. 2a and Fig. 2b, linear regression analysis were performed to fit the rate of precipitation change α using Eq. (1). The result shows that all α's in both P_{99} and P_{50} are lower than 6.8 %/℃ which is the characteristic one at 25 ℃, and the α's in P_{99} are greater than the ones in the P_{50} events. This can tell us that the extreme precipitation will be more extreme than the general one with respect to the same amount of temperature rise. In Fig. 2c the higher *SWI* can be clearly attributed to higher *TPW* in the P_{99} events, but not to hourly precipitation. But, in Fig. 2d it exists no obviously positive proportionality among P_{50}, *SWI*, and *TPW*. Then, in Fig. 2e a maximum negative *HDIV* is found in the event with the maximum *SWI*. However, Fig. 2e and Fig. 2f. show no evident relationship among *HDIV* and the changes of snake lines of the P_{99} and P_{50} events. Finally, in Fig. 2g greater values of *SWI* and *P* are clearly attributed to higher air temperature on the ground surface. In the 99-th percentile, the highest snake line scaling refers to the RCP8.5 scenario, and the lowest one for SPA. This infers that *SWI* can be much enlarged in the scenario of RCP8.5 than SPA. Then, the scaling of snake lines of the P_{99} events are lower than the ones in the P_{50} events. However, as P_{50}'s are quite lower than P_{99}'s, the value of *SWI* will never be much enlarged to exceed the one of the 99-th percentile. So far, we have examined the condition in a local scale on a single mesh, and we next zoom out our focus to investigate the results in a regional scale.

Fig. 3 shows the spatial and frequency distributions of CC scaling α's from all RCM5 members of the P_{99} and P_{50} events. In each percentile, any differences of frequency distribution among the present and future climate projections are not evident. In the P_{99} events there are only 3% of meshes whose CC scaling is less than 6.8 %/℃, and the rest of meshes have greater scaling rate in an average of 1.5

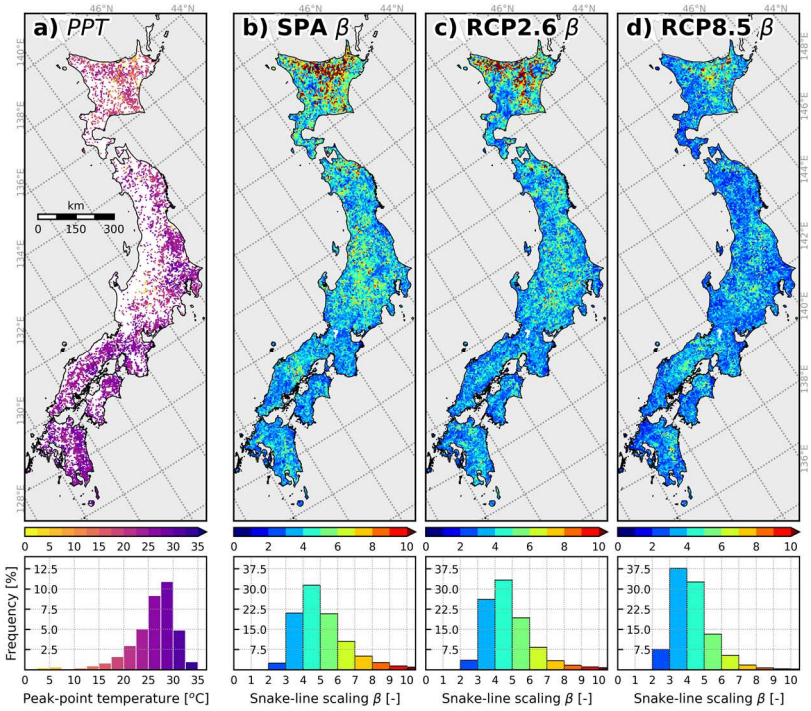

Fig. 4 Spatial and frequency distribution of a) peak-point temperature and b)-d) scaling of change of snake lines obtained from all members of 5-km NHRCM. In a) white patches denote no peak-point temperature being detected by the proposed methodology.

times of amplification with respect to 6.8 %/℃. On the opposite, in the P_{50} events there are less than 15% of meshes which have greater scaling rate, but others are in lower scaling rates ranging from 0.5 to unity.

As for spatial distribution, in the P_{99} events higher scaling rates are distributed along the Japanese Sea Side and some southern regions. In particular, there are lower rate in Osaka bay area, Kanto plain, and mountainous area in east Japan and Hokkaido. To our surprise, there are wider area that has a scaling rate under the scenario of RCP8.5 lower than the one under SPA. More analysis will be required here for reasoning this particular condition. On the other hand, in the P_{50} events only in some small area in Chubu Mountains, there are meshes with higher scaling rates, but others are all in rates lower than 6.8 %/℃. In some inland area the scaling rates are even lower. One common point for the meshes with lower scaling rate is that all these area are almost located in the place at higher altitudes.

3.3 Peak-point Temperature and Snake Line Scaling

As is explained, approximate constant CC scaling may break at a certain temperature, which is called peak-point temperature or *PPT*. It is necessary to find out this temperature before correctly applying CC scaling. Fig. 4a shows the distribution obtained by examining all RCM5 members. To gentle remind, the white patches denote the location without successful detection of *PPT* by using the methodology we proposed. The result shows that *PPT* is higher in the Pacific Ocean Side and becomes lower in the north. It has to be emphasized that our analysis method is highly dependent on extracted data of the effective rainfall events. The result may need more verification with the help of other atmospheric variables.

Fig. 4b to Fig. 4d show the distribution of scaling of snake lines from RCM5 members. The large portion of meshes have the scaling rates greater than 3.0. It can be observed that the scaling in RCP8.5 lower than other members. From the frequency distributions, the overall scaling β in the scenario of RCP8.5 is lower than RCP2.6 and SPA. This can also explain by the distribution. Besides, the area with the quite high scaling rates are almost distributed in Hokkaido. Regarding the distribution

of mesh with low scaling rate, it can be found that the coast area usually has lower rate. It also requires more analysis to resolve this particular condition. To remind again, the rate of snake line scaling can only interpret the relative change ratio of *SWI* to *P* with respect to air temperature change, it cannot give for any absolute value.

4. Conclusions

We investigated the applicability of the Clausius-Clapeyron scaling on quantifying the changes of snake line pattern under the climate change influences. The key advantage of this study is to propose a new approach to physically estimate the relative change of the maximum range of snake line based on the change of air temperature on the ground surface, which can be straightforwardly linked with atmospheric conditions regarding climate change influences. In the current research, the long-term meteorological observation by ground gauges at Kobe weather station was used to successfully verify the applicability of the proposed approach. Also, the climate projections of RCM5 were then used for examining the future change of CC scaling as well as snake line scaling in the Japanese archipelago.

As a constant CC scaling is well but only suited to estimation of precipitation change under general atmospheric thermal conditions in a wider spatial scale, it may not be capable of soundly interpreting nonlinear mechanism of local storm system which is one of frequent types of rainfall triggering sediment disasters. Beyond the main interest of the present study, it is expected that more physical parameters are necessary for clarifying this unresolved nonlinearity of local storm.

However, one concern has to be considered here. Comparing with the high-resolution precipitation observation using XRAIN, the observation of air temperature is still point-wise and insufficient for covering all hazardous rainfall events. This means that some of disastrous rainfall events may not have direct temperature observation data. This shortage of data coverage would currently be the major difficulty to verify the scaling method proposed in this research. It is believed that this demerit can be resolved and overcome once having collected sufficient historical disastrous rainfall events with corresponding temperature observation.

Nevertheless, the scaling of snake line could provide us a quantitative way to estimate the change of snake line patterns in terms of air temperature change under climate change influences. This study could provide a new direction for improving the practice of monitoring of sediment disasters in a changing climate by physically considering atmospheric influences.

Acknowledgements

This work was supported by the Integrated Research Program for Advancing Climate Models (TOUGOU) Grant Number JPMX-D0717935498 from the Ministry of Education, Culture, Sports, Science and Technology (MEXT), Japan and by JSPS KAKENHI Grant Number 22K04331. The authors appreciate MLIT Sabo Planning Division, prefectural governments, and Japan Weather Association (JWA) for sharing valuable datasets.

References

Hayashi, S.-I., Kunitomo, M., Mikami, K. and Suzuki, K. (2022): Recent and Historical Background and Current Challenges for Sediment Disaster Measures against Climate Change in Japan, Water, Vol. 14, No. 15, 2285.

MLIT (2005): Guideline for Determination of Rainfall Threshold for Early-Warning of Sediment Disasters, MLIT, Japan

Mori, N., Takemi, T., Tachikawa, Y., Tatano, H., Shimura, T., Tanaka, T., Fujimi, T., Osakada, Y., Webb, A. and Nakakita, E. (2021): Recent nationwide climate change impact assessments of natural hazards in Japan and East Asia. Weather Clim. Extrem., Vol. 32, 100309.

Murata, A., Sasaki, H., Kawase, H., Nosaka, M., Oh'izumi, M., Kato, T., Aoyagi, T., Shido, F., Hibino, K., Kanada, S., Suzuki-Parker, A. and Nagatomo, T. (2015): Projection of future climate change over Japan in Ensemble Simulations with a High-Resolution Regional Climate Model, SOLA, Vol. 11, pp. 90-94.

Nakakita, E., Hashimoto, G., Morimoto, K. and Osakada, Y. (2018): An influence of atmospheric

stabilization and vapor invasion on occurrence frequency of Guerilla-heavy rainfall, Journal of Japan Society of Civil Engineers, Ser. B1 (Hydraulic Engineering), Vol. 74, No. 5, pp. I_25-I_30.

Nakakita, E., Osakada, Y. and Wu, Y.-H. (2021): Influences of Climate Change, KASEN(Rivers), No. 898, pp. 8-12.

Nayak, S., Dairaku, K., Takayabu, I., Suzuki-Parker, A. and Ishizaki. N. (2018): Extreme precipitation linked to temperature over Japan: current evaluation and projected changes with multi-model ensemble downscaling, Clim. Dyn., Vol. 51, pp. 4385-4401.

Osanai, N., Shimizu, T., Kuramoto, K., Kojima, S. and Noro, T. (2010): Japanese early-warning for debris flows and slope failures using rainfall indices with Radial Basis Function Network, Landslides, Vol. 7, pp. 325-338.

Sasaki, H., Murata, H., Hanafusa, M., Oh'izumi, M. and Kurihara, K. (2012): Projection of Future Climate Change in a Non-Hydrostatic Regional Climate Model Nested within an Atmospheric General Circulation Model, SOLA, Vol. 8, pp. 53-56.

Utsumi, N., Seto, S., Kanae, S., Maeda, E. and Oki, T. (2011): Does higher surface temperature intensify extreme precipitation? Geophys. Res. Lett., Vol. 38, L16708.

Westra, S., Fowler, H.J., Evans, J.P., Alexander, L.V., Berg, P., Johnson, F., Kendon, E.J., Lenderink, G. and Roberts, N.M. (2014): Future change of the intensity and frequency of short-duration extreme rainfall, Rev. Geophys., Vol. 52, pp. 522-555.

Wu, Y.-H., Nakakita, E. and Yamaji, A. (2020): Future change of rainfall-triggered land-slide risk using NHRCM05 based on critical line method, Journal of Japan Society of Civil Engineers, Ser. B1 (Hydraulic Engineering), Vol. 76, No. 2, pp. I_67-I_72.

Wu, Y.-H., Nakakita, E. and Yamaji, A. (2021): Future change of snake line pattern and its relation to sediment disasters, Journal of Japan Society of Civil Engineers, Ser. B1 (Hydraulic Engineering), Vol. 77, No. 2, pp. I_193-I_198.

(Received August 31, 2022)